
Bioceramics

COPYRIGHTED MATERIAL

ONE-STEP PREPARATION OF ORGANOSILOXANE-DERIVED SILICA PARTICLES

Song Chen,¹ Akiyoshi Osaka,^{*1} Satoshi Hayakawa,¹ Yuki Shirotsaki,¹ Akihiro Matsumoto,¹ Eiji Fujii,² Koji Kawabata,² Kanji Tsuru^{1§}

¹Graduate School of Natural Science and Technology, Okayama University
Okayama-shi, 700-8530 Japan

²Industrial Technology Center of Okayama Prefecture, Okayama-shi, 701-1296 Japan

[§]Now at Faculty of Dental Science, Kyushu University, Fukuoka, 812-8582, Japan

*E-mail: a-osaka@cc.okayama-u.ac.jp

ABSTRACT

Silica particles and their derivatives with meso-structure attracted much attention, but they were synthesized through complicated multi-step procedure. Considering biomedical application, no surfactants, used in almost all cases above, should be employable due to fear of their toxicity. The present study explored one-step sol-gel preparation of silica particles with biomedical functionalities, starting from Stöber-type systems, and characterized by Transmission Electron Micrograph or ²⁹Si MAS NMR spectroscopy. The Ca-containing particles, derived from the precursor system tetraethoxysilane (TEOS)-H₂O-C₂H₅OH (EtOH)-CaCl₂-NH₄OH, consisted of primary particles of ~ 10 nm, and were spherical in shape with the diameter of ~ 1000 nm, where Ca bridged Si-O- on the opposite particle surface. In contrast, the Ca-free particles were smaller with 400 ~ 500 nm in size due to the absence of such bridging effects. In addition, the Ca-containing ones deposited petal-like apatite within one week in Kokubo's simulated body fluid (SBF), which was interpreted in terms of the Ca release from the particles. Amino-modified silica particles were derived from the sol-gel precursor system aminopropyltriethoxysilane (APTES)-TEOS-H₂O-EtOH where APTES behaved not only as the catalyst but also a reactant; i.e., this was a self-catalyzed sol-gel system. Hydrogen bonding among the amino group of APTES on one particle surface and with Si-O- on the other was suggested to work in agglomeration of the primary particles. Bovine serum albumin was covalently fixed on the APTES-silica surface, suggesting their applicability of proteins or other growth factor delivery.

INTRODUCTION

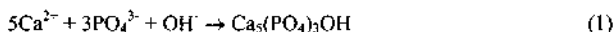
Sol-gel derived SiO₂ is similar to melt-quenched silica glass in random siloxane bridging network (>Si-O-Si<) but different in involving much free silanol groups (Si-OH) in the amorphous lattice. Moreover, their preparation routes mostly involved some templates or surfactants which might be toxic and inadequate for biomedical applications.¹⁾ A few groups then prepared sol-gel silica particles from simple system like tetraalkoxysilane-ethanol (EtOH)-H₂O, where tetraalkoxysilane included tetramethoxysilane or tetraethoxysilane (TEOS). For example, Kortessuo prepared silica xerogels (dry-gels without calcination) from the system TEOS-polyethyleneglycol-H₂O-CH₃COOH and explored their ability of delivering toremifene citrate.²⁾ Kneuer et al.³⁾ proposed organo-modified hybrid silica particles, or amino-functionalized silica particles, as DNA carriers, where *N*-(2-aminoethyl)- or *N*-(6-aminoethyl)-3-aminopropyltrimethoxysilane was employed for introducing amino-functionality. Such application of sol-gel silica is recognized because of good biocompatibility of Si-OH groups.^{4,5)} No significant adverse effects are observed when those silica materials are applied in the human body. Rather, silicate components eluted in the surrounding medium were found to stimulate several genes,⁶⁾ or those remaining in the gel body favored cell proliferation.⁷⁾ As particle size effects are taken into account, the silica gel particles, small enough (~10 μm), are more convenient and attractive, because they can be directly introduced by injection into human tissues as Shirotsaki et al. demonstrated with ceramic particles dispersed in hydrogels.⁸⁾ Especially, particles less than 500 nm in size are highly likely endocytosed by the living cells, and the therapeutic drugs held by them are

directly released into the cells. Moreover, such injection route deserves the lowest level of tissue invasion that contributes to the patients' comfort.

By virtue of the above advantages, various silica particles with solid, porous, and hollow structures have been prepared and applied in, *e.g.*, drug delivery system⁹⁾ and immunosassy.¹⁰⁾ Their size, morphology, and homogeneity could be well controlled by means of the conventional sol-gel route. However, lower chemical reactivity of the Si-OH groups with functional groups like -NH₂ or -COOH groups hardly led to direct covalent bonds with biologically active proteins, enzymes or anti-body, if the silica particles were simply mixed or in contact with their solutions. Consequently, the loading efficiency of those biological factors was very low if only the physical absorption was predominant. Therefore, actually, most applications are related to the functionalized silica particles, not the naked or original silica particles.

Among possible agents for surface modification of silica, aminosilanes seem most attractive and important, because their -NH₂ groups could be reacted with the -COOH groups of enzymes or other peptides to form amide bonds, or form RGD peptides (R: arginin, G: glycine, and D: aspartic acid peptides) via cross-linking with, for example, carbodiimide (EDC).¹¹⁾ What is more, no additional catalytic additives should be needed when aminosilanes like aminopropyltriethoxysilane (APTES) are involved in the precursor systems. That is, with such silanes pH of the systems becomes alkaline enough to initiate hydrolysis and condensation reactions of the relevant components, which may lead to silica nanoparticles similar to those in the Stöber-type systems. In the conventional route, amino-modified silica particles will be prepared in two-steps: the preparation of silica particles, and the aminosilane modification of the resultant silica particles. After Li et al.,¹²⁾ successful incorporation of APTES depended on high amount of Si-OH groups. The silica nanoparticles were commonly treated with "Piranha solution" (H₂SO₄/H₂O₂) or HNO₃ to introduce high amount of Si-OH groups and then refluxed in the APTES/toluene solution for a few hours. Such route is complex and dangerous since "Piranha solution" is very corrosive and toluene is also toxic. The exploration of novel and concise route for such modification is necessary.

An advantage of the Si-OH groups or hydrated silica layers to serve nucleation sites for biologically active apatite has been commonly described in the literature. For example, Li et al.¹³⁾ pointed out that pure silica gels via a sophisticated sol-gel route developed by Nakanishi et al.¹⁴⁾ deposited apatite layer in the Kokubo's simulated body fluid (SBF)¹⁵⁾ that had the same inorganic ion components as the human blood in similar concentration. Such apatite layers exhibit good affinity with bone tissue, and hence accelerate recovery of bone defects. Thus, the Si-OH containing silica particles might deposit the bioactive apatite when soaked in SBF and can be used as bioactive fillers. Unfortunately, the rate of apatite deposition was very low if only Si-OH groups existed.¹⁶⁾ Tsuru et al.¹⁷⁾ found that Ca(II) released from the silicate materials could significantly increase the super-saturation degree of SBF and promoted bioactive apatite deposition, pushing the equilibrium (eq. (1)) toward apatite formation.



Thus, apatite could reasonably be deposited on Ca(II)-involved silica particles. Moreover, as in silicate glass or crystals, calcium ions are expected to bridge adjacent 'O-Si< units, >Si-O⁻••Ca²⁺••O-Si<, which may control the particle size of the resultant silica.

On the above bases, the one-step sol-gel method was applied in the modified Stöber sol-gel precursor system to yield two functionalized silica particles: Ca-free and Ca-containing silica particles and amino-functionalized silica particles. The Ca-containing ones were derived from the precursor solution in the system TEOS-H₂O-EtOH-CaCl₂-NH₄OH, while the amino-functionalized ones were derived from the system TEOS-APTES-EtOH-H₂O. Apatite formation on the particles in SBF was

examined with X-ray diffraction or with scanning and transmission electron micrographs. Bovine serum albumin (BSA) was also fixed on the amino-functionalized silica particles. Mechanisms of secondary particle formation and particle size change as well as effects of amino groups were discussed.

EXPERIMENTAL

Preparation of the Ca-containing and amino-functionalized silica particles

The Ca-containing silica particles were prepared from the modified Stöber precursor system¹⁸⁾ TEOS-EtOH-H₂O-NH₄OH-CaCl₂. CaCl₂ and TEOS solutions were prepared beforehand: CaCl₂ aqueous solution and TEOS/ethanol solution. Appropriate amounts of CaCl₂ (0 ~ 0.15 mmol) were dissolved in 389 mmol of water to obtain CaCl₂ aqueous solutions with various concentrations. The TEOS/ethanol solution was obtained by adding 12 mmol of TEOS into 120 mmol ethanol. Those two solutions were mixed in varied ratios to prepare precursor solutions, held in tightly capped one-necked flasks (50mL), which were then transferred in an ultrasonic bath. As soon as 3 mL of 28mass% ammonium hydroxide solution was added to initiate the hydrolysis and condensation of TEOS, the reaction mixture was irradiated with an ultrasound for 30 min at room temperature to produce opaque suspension. The resultant particles were separated by centrifugation at 3,500 rpm for 5 min, and then washed with water for 3 times before dried at 105 °C overnight. Table I shows typical two compositions of starting materials and pH in the precursor solutions.

Table I. The starting systems similar to Stöber et al.¹⁸⁾ and pH in the precursor solutions.

Samples	CaCl ₂ (mmol)	TEOS (mmol)	H ₂ O (mmol)	EtOH (mmol)	pH
Silica	0	12	389	120	12.5
Ca-Silica	0.05	12	389	120	12.5

The amino-functionalized silica nanoparticles were prepared from the precursor system TEOS-EtOH-H₂O-APTES using a novel one-step sol-gel route, as originally proposed by Chen et al.¹⁹⁾ Unlike ammonia in the above Stöber precursor system, here, APTES not only provided the functional amino groups but also served as the base self-catalyst. Both APTES (0, 0.45, and 4.5 mmol) and TEOS (4.5 mmol) were mixed in the ethanol (440 mmol)/water (280 mmol) solution, held in 50-mL one-necked flasks at room temperature. The mixture was kept stirring for 1 h. Like in the above Stöber sol-gel system,¹⁸⁾ the hydrolysis and condensation of the silanes gave opaque suspension. The resultant particles were collected by centrifugation at 2,500 rpm for 5 min, washed with water 3 times, and then dried at 105 °C overnight. Table II shows the compositions of the starting materials and pH in the starting solution. Both systems above involved water in great excess over the stoichiometric amount to fully hydrolyze all ethoxy groups into silanol ones: >Si-OEt → >Si-OH.

Table II. The starting systems for the amino-modified silica, and pH in their precursor solutions.

Samples	APTES (mmol)	TEOS (mmol)	H ₂ O (mmol)	EtOH (mmol)	pH
AMSi0	0	4.5	280	440	6.9
AMSi045	0.45	4.5	280	440	10.9
AMSi45	4.5	4.5	280	440	11.2

Characterization

Size and morphology of the samples were observed under a field-emission type scanning electron microscope (FE-SEM, JSM-7500, JEOL, Japan). Infrared spectra were taken on a Fourier transform infrared spectrometer (FT-IR, Model 300, JASCO, Japan) using the KBr pellet method.²⁹⁾ Si magic

One-Step Preparation of Organosiloxane-Derived Silica Particles

angle spinning (MAS) nuclear magnetic resonance (NMR) spectra and cross-polarization (CP)-MAS NMR spectra were recorded with a Fourier transform (FT)-NMR spectrometer (UNITYINOVA300, Varian, Palo Alto, CA, USA) equipped with a CP-MAS probe.

The Ca-release and Si-release characteristics were measured for the Ca-containing silica particles where 10 mg particles were soaked in 10 mL of saline, whose pH was adjusted to 7.4 at 36.5 °C with tris-(hydroxymethyl)aminomethane (Tris, 50 mM) and 1 mol/L HCl. Every other day, the particles were collected by centrifugation at 3,500 rpm for 5 min. The Ca(II) and Si(IV) concentration of the supernatant was measured by inductively coupled plasma emission spectroscopy (ICP, SPS-7700, Seiko, Japan). Both Ca-free and Ca-containing silica particles were soaked in 30 mL SBF at 36.5 °C up to 7 d, and then collected every other day by centrifugation at 3,500 rpm for 5 min. After rinsing with water, the particles were dried at 105 °C and their structures were further examined by thin film X-ray diffractometry (TF-XRD, model RAD IIA, Rigaku, Tokyo; Cu α , 30kV-20mA) as well as scanning electron micrograph (FE-SEM; S-4700, Hitachi, Tokyo) and transmission electron micrograph (TEM; JEM-2010, JEOL, Tokyo).

Bovine serum albumin (BSA) was fixed on AMSi045 and AMSi45. Prepared was aqueous solution (20 mL) involving 1-ethyl-3-(3-dimethylaminopropyl)carbodiimide hydrochloride (EDC, 50 mg) and N-hydroxysuccinimide (NHS, 50 mg), to which BSA and the particles, 20 mg each, were added. After the mixtures were stirred for 24 h at room temperature, the silica particles were separated from the solution by centrifugation at 2,500 rpm for 5 min, washed with water 3 times, and finally dried at 60 °C overnight.

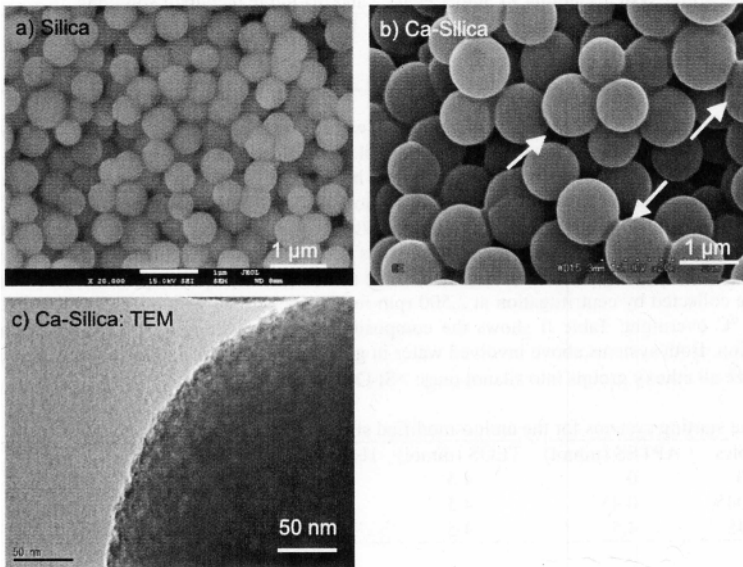


Fig. 1. FE-SEM images of (a) silica particles and (b) Ca-silica particles; (c) a TEM image of a Ca-silica particle (Table I). The arrows in (b) show surface irregularities (necking and defects).

RESULTS

Ca-containing silica particles: microstructure and apatite deposition

The resultant silica particles were spherical in shape. The FE-SEM images in Fig. 1 show that the Ca-free silica particles (Fig. 1a) were 400 ~ 500 nm in diameter, while the Ca-containing ones (Fig. 1b) were 800 ~ 1000 nm. Fig. 1c shows a typical TEM image of the Ca-silica sample in Table I; as the Ca-silica image indicates, the particles found in the SEM images consisted of much smaller primary particles (~10 nm). Similar TEM images were taken for other samples from the systems with larger CaCl₂ contents in the present study. Size distribution profiles for the secondary particles, not shown here, taken with a Particle size analyzer (Honeywell, UPA-150, Microtrac Inc., USA) were centered at 500 nm with ~200 nm width (at half height maximum) for the Ca-free silica, and centered at 900 nm with 300 nm width for the Ca-silica particles. Those data well agreed with the SEM images in Fig. 1. It is thus indicated that the addition of Ca(II) in the starting solution favors the growth of the secondary particles. The image in Fig. 1b indicates that some particles were slightly fused together, showing a little crater-like surface defect (arrows).

Fig. 2 shows the FT-IR spectra of (a) silica particles and (b) Ca-containing silica particles. No significant differences were found between spectra (a) and (b), and this confirmed that both particles consisted of similar molecular groups. The broader peak around 3430 cm⁻¹ was assigned to the stretching vibration of O-H in the >Si-OH groups and the adsorbed water molecules, which also give a small but sharp one at 1640 cm⁻¹. The strongest one at 1111 cm⁻¹ and a smaller one at 806 cm⁻¹ was $\nu(\text{Si-O})_{\text{asym}}$ and $\nu(\text{Si-O})_{\text{sym}}$ due to the Si-O-Si bonds, while the bands at 960 cm⁻¹ were assigned to Si-OH groups. The strongest peak at 1111 cm⁻¹ in both spectra indicated the present particles, regardless of the presence of Ca(II), had similar silicate networks and most Si-OH groups have condensed into Si-O-Si groups. Indeed, both yielded very similar ²⁹Si MAS NMR spectra (not presented here), that is, they had similar distribution in Qⁿ groups, Q⁴/Q³/Q² = 70/28/2 in mol % for the Ca-free silica, and 69/30/1 for the Ca-silica: here n stands for the number of bridging oxygen atoms in a SiO₄ tetrahedron.

Fig. 3(a) plots the release profile of Ca(II) for the Ca-silica particles and (b) represents that of Si (IV) for both Ca-free silica and Ca-silica when the corresponding silica samples were soaked in saline solution. In (a), least square fitting curves were indicated, assuming that the Ca(II) release proceeded in diffusion-controlled and reaction controlled mechanisms: Diffusion model: [Ca] ≈ 0.013 d^{1/2} (χ² = 4.5 × 10⁻⁵); Reaction model: [Ca] ≈ 0.0055 d (χ² = 1.5 × 10⁻⁵). Empirically, the concentration of Ca(II) increased with the soaking time to confirm the involvement of Ca(II) in the Ca-silica particles. Yet

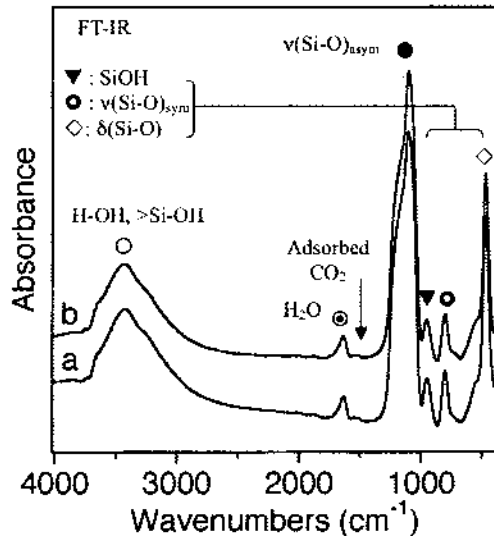


Fig. 2. The Ca-free silica particles (a) and Ca-silica particles (b) gave basically same FT-IR profiles.

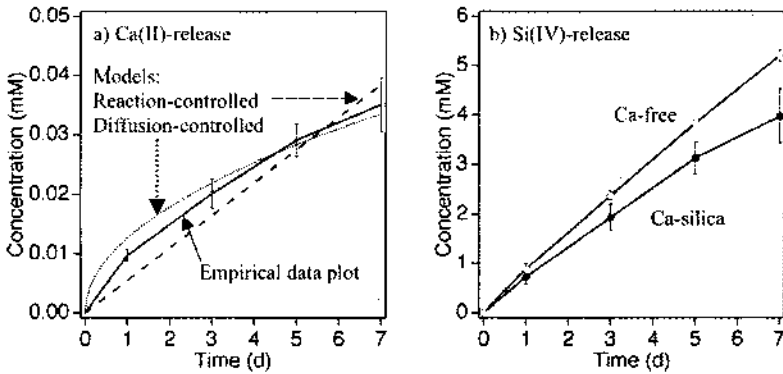


Fig. 3. (a): Ca(II) release profile for the Ca-silica particles. The release profiles due to reaction- and diffusion-controlled mechanism are also plotted. (b): Si(IV) profile for silica and Ca-silica.

either model could not well reproduce the empirical data plot. Fig. 3(b) shows a slight difference in Si(IV) release between the Ca-free silica and Ca-silica samples, responsible to the Ca(II) involvement. The observation is relevant to the secondary particle microstructure and degradation of the secondary particles, which are to be discussed later.

Although increase in Ca(II) stimulates apatite precipitation¹⁷⁾ (eq. (1)), the present Ca-silica is inferior in apatite-forming activity as relatively small amounts of Ca(II) got into saline (Fig. 3(a)). Fig. 4(left) shows the XRD patterns of the Ca-free silica particles (a) and the Ca-containing silica particles (b) after both were soaked in SBF for one week. The Ca-free silica particles showed no sign of apatite deposition, but only exhibited an amorphous XRD profile, except a faint peak at 31° (arrow). In contrast, the Ca-containing silica particles gave two weak but distinct peaks at 26° and 32° in profile

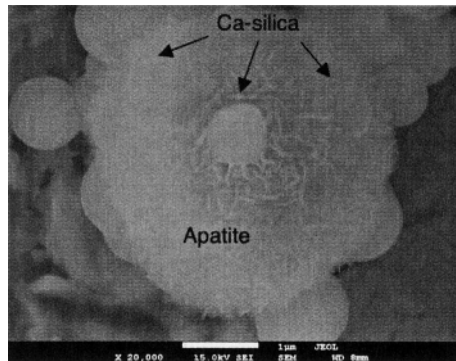
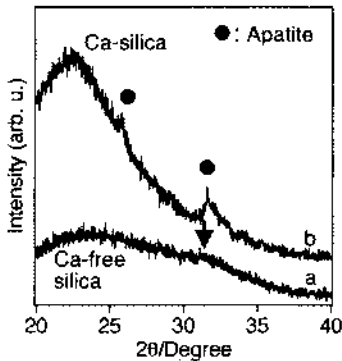


Fig. 4. (Left) XRD pattern of the Ca-free silica particles (a) and Ca-silica particles (b) after soaked in SBF for 7 d. See text for the arrow.

Fig. 5. (Right): a FE-SEM image of the Ca-silica particles after soaked in SBF for 7 d, with petal-like apatite crystallites. Bar: 1 µm.

(b). The 26° peak was assigned to the (002) diffraction and the 32° one was due to the envelope of the (211), (112) and (300) diffractions of apatite.^{13,14,16,17} Although the peak intensity was lower than that for common materials with the apatite depositing ability,^{13,14,16,17} the SEM photograph of the Ca-silica particles soaked in SBF for 7 (Fig. 5) shows petal-like crystalline deposits, with the same morphology as those apatite particles on those materials above. Those crystallites looked embracing the silica particles. From those results, the Ca-containing silica particles are surely active to be fixed with living bone when embedded in the bone tissues.

Amino-functionalized silica particles: microstructure and protein immobilization

The FE-SEM images of the particles AMSi045 and AMSi45 in Figs. 6 (a) and (b), respectively, illustrates some differences among them in size and morphology. The particles of both samples were spherical but they were largely fused together, which gives an impression that those are much more agglomerated than the previous Ca-free and Ca-silica. Yet, the component particles of AMSi045 remain more particle-like than those of AMSi45 which show highly fused peanut-shell morphology. That is, increase in APTES brought greater degree of agglomeration. The individual particles for AMSi045 seemed larger in diameter (300 ~ 400 nm) than those for AMSi45 (200 ~ 300 nm), though high irregularity in shape prevents definite measurement of the size. Moreover, the surface of AMSi45 particles appeared rougher than that for AMSi045. The TEM observation indicated that both samples consisted of ~ 10 nm primary particles. It was noted in the course of preparation that, at the lower APTES amounts (*e.g.*, 0.45 mmol), the reaction in the precursor solution was quite mild and the opaque suspension was obtained after 30 min. In contrast, at the higher APTES amounts (> 0.45 mmol), the reaction in the precursor solutions became very vigorous and white sediments precipitated on the wall and at the bottom of the flask within few min. Such reaction conditions lead to the difference in agglomeration detected above.

Though they showed a little difference in morphology,²⁹Si MAS NMR spectra indicated that both samples had very similar structural constitution in terms of the fraction of Tⁿ and Qⁿ units. Fig. 7 shows the ²⁹Si MAS NMR spectrum of AMSi045, and a similar one was obtained for the other sample. The NMR spectrum was extended in two regions, -80 ~ -120 ppm for Qⁿ units and -40 ~ -80 ppm for Tⁿ ones. The Gaussian fitting after Carroll et al.²⁰ was employed to deconvolute the profile into five clear peaks, *i.e.*, T² units NH₂(CH₂)₃Si(-O-Si)₂(OH) at -58 ppm, T³ units NH₂(CH₂)₃Si(-O-Si)₃ at -66 ppm, Q² units Si(-O-Si)₂(OH)₂ at -90 ppm, Q³ units Si(-O-Si)₃(OH) at -100 ppm, and Q⁴ units Si(-O-Si)₄ at -109 ppm. The presence of both T and Q units confirmed that the hydrolysis and

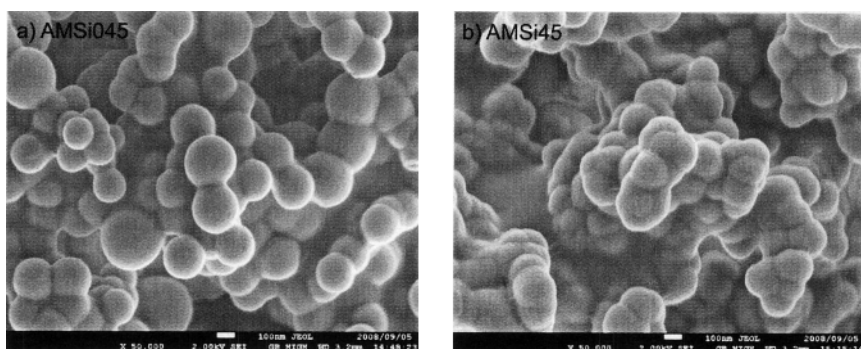


Fig. 6 FE-SEM images of the particles AMSi045 (a) and AMSi45 (b). (Bar: 1 μ m)

condensation of APTES and TEOS took place in the precursor solutions. The strongest intensity of both Q³ and Q⁴ units and the medium one of T³ indicated that most Si-OH in the particles have condensed into the siloxane network bonds (Si-O-Si).

BSA fixation is confirmed by detecting vibrational bands characteristic of proteins and the cross-linking agent EDC. Fig. 8 shows the FT-IR spectra for AMSi045 and its derivatives. Spectrum (a) for AMSi045 had the bands for the silica network at 1070 and 800 cm⁻¹, assigned to $\nu(\text{Si-O})_{\text{asym}}$ and $\nu(\text{Si-O})_{\text{sym}}$. A shoulder peak at 960 cm⁻¹ was due to the Si-OH groups, which was detected in Fig. 2 as an independent peak for Ca-free and Ca-silica. The broader band extending from 2800 to 3500 cm⁻¹ was due to -OH of >Si-OH and adsorbed H₂O, which gave a sharper structure in Fig. 2. The distinct -NH₂ peak at 1543 cm⁻¹ shows the presence of APTES in AMSi045. It follows the result from the above ²⁹Si NMR spectrum. In addition, both peaks at 2941 and 2873 cm⁻¹ were attributed to -CH₂ groups or methylene skeleton introduced by APTES. Spectra (b) and (c) for the samples after contact with the BSA solution indicate a few IR bands related to BSA whose IR spectrum was represented as (d). Of the spectra for two AMSi045 samples, spectrum (b) showed no additional bands other than those found for the silica structure. On the other hand, spectrum (c) for the sample treated with EDC together with APTES gave a doublet band with medium intensity characteristic of amide bonds, which was commonly denoted as amide I (~1680 cm⁻¹) and amide II (~1590 cm⁻¹), and both were basically due to a C=O stretching vibration, $\nu(\text{C}=\text{O})$. A trace peak at 3305 cm⁻¹ was assigned to -N-H bonds of BSA that was absent in spectrum (a) or (b) in Fig. 8. Those results indicate that BSA was immobilized on the particle

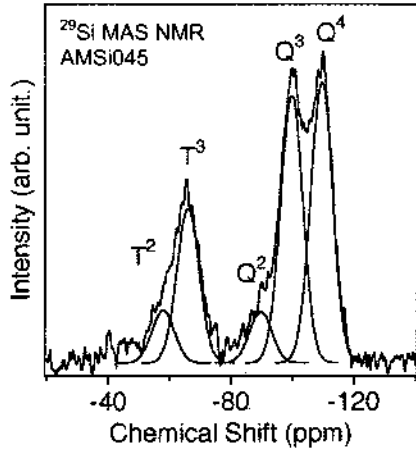


Fig. 7. A ²⁹Si MAS NMR spectrum for AMSi045. Each component peak was derived from Gaussian deconvolution.²⁰⁾

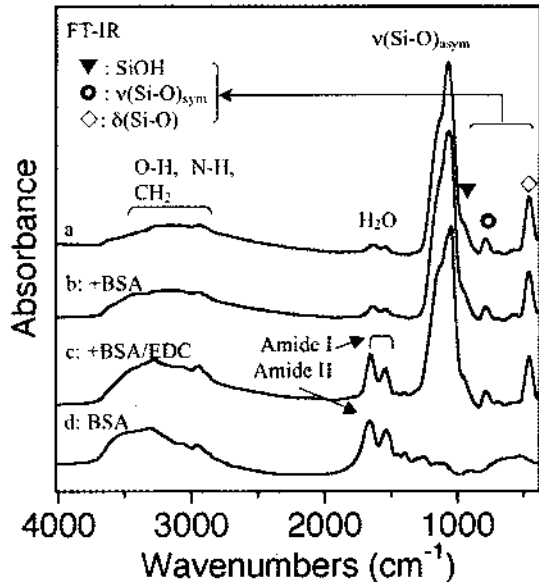


Fig. 8. FT-IR spectra of AMSi045 (a), AMSi045 after soaked in the BSA solution without EDC (b) and with EDC (c) as well as BSA (d).

surface as EDC was employed as an effective cross-linker. It agrees with the results from Szurdoki²¹⁾ and Mao²²⁾ who used EDC as the cross-linker for proteins and natural polymers.

DISCUSSION

Ca-containing silica particles: formation mechanism and apatite deposition

Bogush and Zukoski,^{23,24)} considered that the Stöber silica particles consisted of ~ 10 nm primary particles, and Green et al.²⁵⁾ proposed the microstructure as they measured small-angle X-ray scattering. From Table 1, the reaction solution was basic with pH 12.5. The silanol groups have an isoelectric point of about 2 ~ 3,²⁶⁾ and hence, in such alkaline solution, they should be in the forms of hydrated $>SiO^-(aq)$. As they were un-polymerized, almost all of those units remained on the primary particle surface, yielding a negatively charged hydrated layer. The layer then causes repulsive interactions among the adjacent primary particles, but the $>SiO^-(aq)$ forms strong hydrogen bonds with the water molecules. This overwhelms the repulsion to agglomerate the primary particles to SEM observable larger secondary particles.

The presence of $CaCl_2$ in the starting solutions stimulated the secondary particle growth; ~500 nm for the Ca-free particles and ~ 1000 nm for the Ca-silica ones. Zerrouk et al.²⁷⁾ studied the interfacial behavior of mono-disperse (~15 nm) silica sols in terms of their surface charge as a function of pH and salt concentration. They proposed the concept of Ca^{2+} coagulation critical concentration in the range pH 7.5~9, assuming that $Ca(II)$ promoted the agglomeration. In the present study, pH of the starting solution well exceeded their range but was 12.5. Since the higher was pH, the more $>SiO^-(aq)$ yielded, one would expect even smallest amount of $Ca(II)$ should form $>Si-O^-\cdot\cdot Ca^{2+}\cdot\cdot O-Si<$ links. Thus, it is reasonable to suggest that the Ca^{2+} ions also contributed to the agglomeration of the ~ 10 nm primary particles. If like this, the $Ca(II)$ must be involved in the silica particles. Indeed, the release curve of $Ca(II)$ in Fig. 3(a) confirmed it. Fig. 9 compares the ^{29}Si CP-MAS NMR spectra for the Ca-free silica and Ca-silica samples.²⁸⁾ Under the cross-polarization (CP) mode, the nuclear magnetic moment energy of H is transferred to another nuclei in the neighborhood. Thus, the drastic decrease in NMR intensity due to the $Ca(II)$ incorporation means that almost all Si atoms in the Ca-silica were relatively far apart from H than in the Ca-free silica. This means very little amount of $>Si-OH$ or H_2O molecules was present among the primary particles or in the primary particles themselves. In other words, above results conclude that the calcium ions expelled H from the $>Si-OH$ units (or $Si-O(aq)$ involved in the hydrogen bonds) to form $>Si-O^-\cdot\cdot Ca^{2+}\cdot\cdot O-Si<$ links.

The $Ca(II)$ release then takes place in two mechanisms: one is to be associated with the degradation of the secondary particles due to the hydrolysis of the $>Si-O^-\cdot\cdot Ca^{2+}\cdot\cdot O-Si<$ links, and the other is due primarily to $Ca(II)$ diffusion, associated with the hydrolysis, without degradation of the silica secondary particles. The $Ca(II)$ release profile in Fig. 3(a) has moderately been approximated with either model in Fig. 3, yet the diffusion-controlled model seems better than the reaction-controlled

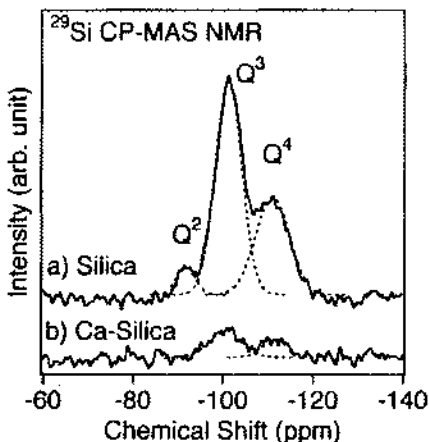
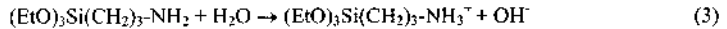


Fig. 9. ^{29}Si CP-MAS NMR spectra for a) the Ca-free silica and b) Ca-silica particles. The calcium involvement drastically decreased the CP-MAS NMR intensity (Chen et al.²⁸⁾)

model in terms of kai-square (χ^2). Diffusion model: $[Ca] \approx 0.013 d^{-1/2}$ ($\chi^2 = 4.5 \times 10^{-5}$); Reaction model: $[Ca] \approx 0.0055 d$ ($\chi^2 = 1.5 \times 10^{-5}$). Moreover, the Si(IV) release was definitely reaction controlled because of the profiles indicated linear dependence on time, though a small deviation was detected for the Ca-silica sample in prolonged contact with saline. After the Pourbaix diagram,²⁹⁾ dissolution of silica as $HSiO_3^-$ practically takes place at pH~10 or higher: with $\log(HSiO_3^-) = -15.21 + pH$, and $\log(HSiO_3^-/H_2SiO_3) = -10.00 + pH$, 0.1mM $HSiO_3^-$ will be attained pH > ~10. In the saline with 7.4 in pH, detectable dissolution unlikely occurs, but, if the presence of Si(IV) is evidenced in Fig. 2, degradation of the secondary particles to liberate primary particles, and this is responsible for the Si(IV) species. In association with the degradation, therefore, the surface layer that involves Ca(II) as bridging the primary particles is to be hydrolyzed, and the calcium ions are liberated from the >Si-O••Ca bonds and diffuse to the top surface. This makes the diffusion-controlled model dominant in the release profile analysis, with keeping some validity of the reaction-controlled model. Yet, detailed study is needed before elucidating a definite conclusion on the mechanism.

Amino-functionalized silica particles: mechanism of formation

The amino group of APTES is susceptible to hydrolysis or protonation, and hence the system becomes basic due to the liberated hydroxyl group as eq. (3):



Indeed, Table 2 showed pH was 10.89 for the precursor system APTES-TEOS-EtOH-H₂O. Under such basic conditions, the OH⁻ ions directly attacked Si atoms having the highest positive charge,³⁰⁾ i.e., the Si atom in the (EtO)₃Si- group of both TEOS and APTES molecules was subjected to coordination expansion, taking 5-fold coordination in the reaction intermediate. Then, the Si atom of APTES has three active sites, like that in alkali disilicate. Since the latter Si(IV) forms an amorphous silicate network or alkali disilicate glass, APTES should form silicate gel particles. TEOS with four-functional Si(IV) is known to yield silica gel bodies. Contrary to the expectation, the present study confirmed that APTES would not form gels. After van Blaaderen and Vrij,³¹⁾ the hydrolyzed APTES tended to form six- or five-membered intra-molecular rings. Such ring formation should, due to their bulkiness, sterically suppress condensation of APTES itself from yielding three-dimensionally grown gels. It is then considered that the formation of amino-modified silica particles requires >Si-OH groups derived from TEOS. In the present alkaline precursor solution, two hydrated species were present: positively charged -NH₃⁺(aq) and negatively charged >Si-O⁻(aq). After Chen et al.,¹⁹⁾ the particle surface was rich in amino groups. The presence of those hydrated ions with opposite charges favors agglomeration of the primary particles due to hydrogen bonding. Fig. 10 schematically represents such interaction leading to the agglomeration. The difference in morphology between AMSi045 and AMSi45 might be attributed to more basic level for the latter system, which would lead to highly vigorous reaction and higher degree of chances in which the >Si-O⁻ and ⁺H₃-R-Si< should be present toward each other on the facing surfaces. Yet, detailed understanding of the agglomeration mechanism

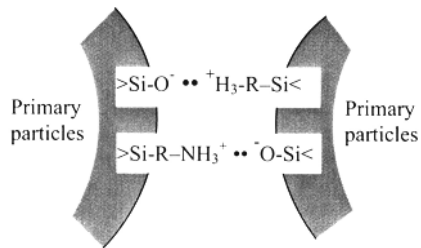


Fig. 10. Two amino-modified silica primary particles are agglomerated via the hydrogen bonding between >Si-O⁻ and ⁺H₃N-R-Si< on the facing surfaces.

should need further study.

CONCLUSION

From one-step sol-gel procedure, two series of silica particles were prepared, i.e., Ca-containing silica and amino-modified silica particles, as well as pure silica particles, from the starting solution systems TEOS-H₂O-EtOH-CaCl₂-NH₄OH for the former silica particles, and from TEOS-H₂O-EtOH-APTES for the latter. The Ca-silica particles were spherical in shape and consisted of ~ 10 nm primary particles. Their size increased with the amount of CaCl₂ in the precursor solutions from 400 ~ 500 nm for the Ca-free silica particles to 800 ~ 1000 nm for the Ca-silica ones. The ²⁹Si MAS NMR analysis indicated that the NMR intensity of the Si atoms was considerably reduced due to the cross polarization, and hence calcium ions formed >Si-O⁻ •• Ca²⁺ •• O-Si<. That bond was considered to bridge the primary particles together, and responsible for the particle growth. Analysis of Si(IV) release into saline indicated that the secondary particles were degraded to liberate the primary particles. The Ca(II) was released dominantly due to the diffusion controlled mechanism since a parabolic approximation fitted better the empirical data. The Ca(II) released from the Ca-silica particles into SBF promoted the deposition of petal-like apatite crystallites within one week. Thus, the Ca-silica particles are applicable to the bioactive fillers for bone regeneration.

In the course of evolving the amino-modified silica particles, APTES worked not only as a reactant but also the catalyst which resulted in pH ~ 11. The FE-SEM image revealed that the particles were spherical in shape less than 500 nm in diameter, consisting of ~ 10 nm primary particles. From the analyses of ²⁹Si MAS NMR spectrum and FT-IR spectra, >Si-O⁻ (aq) groups and ¹H₃-R-Si< (aq) groups were presented on the particle surface, and strong hydrogen bonds formed between them was to promote the agglomeration of the ~ 10 nm primary particles into the secondary particles. Moreover, in the presence of carbodiimide, bovine serum albumin was covalently fixed on the particle surface. Thus, the amino-functionalized silica particles have the high potential applications as carriers for enzymes or DNA.

REFERENCES

- ¹Q.-M. Zhang, K. Ariga, A. Okabe, and T. Aida, A Condensable Amphiphile with a Cleavable Tail as a "Lizard" Template for the Sol-Gel Synthesis of Functionalized Mesoporous Silica, *J. Am. Chem. Soc.*, **126**, 988-989 (2004).
- ²P. Kortesuo, M. Ahola, S. Karlsson, I. Kangasniemi, A. Yli-Urpo, and J. Kiesvaara, Silica Xerogel as an Implantable Carrier for Controlled Drug Delivery—Evaluation of Drug Distribution and Tissue Effects After Implantation, *Biomaterials*, **21**, 193-198 (2000).
- ³C. Kneuer, M. Sameti, E. G. Haltner, T. Schiestel, H. Schirra, H. Schmidt, and C.-M. Lehr, Silica Nanoparticles Functionalized with Aminosilanes as Carriers for Plasmid DNA, *Int. J. Pharm.*, **196**, 257-261 (2000).
- ⁴L. Ren, K. Tsuru, S. Hayakawa, and A. Osaka, Novel Approach to Fabricate Porous Gelatin-Siloxane Hybrids for Bone Tissue Engineering, *Biomaterials*, **23**, 4765-4773 (2002).
- ⁵Y. Shirosaki, K. Tsuru, S. Hayakawa, A. Osaka, M. A. Lopes, J. D. Santos, and M. H. Fernandes, In vitro Cytocompatibility of MG63 Cells on Chitosan-Organosiloxane Hybrid Membranes, *Biomaterials*, **26**, 485-493 (2005).
- ⁶L. L. Hench, Stimulation of Bone Repair by Gene Activating Glasses, *Key Engineering Materials*, **254-256**, 3-6 (2004).
- ⁷K. Deguchi, K. Tsuru, T. Hayashi, M. Takaishi, M. Nagahara, S. Nagotani, Y. Sehara, G. Jin, H. Zhang, S. Hayakawa, M. Shoji, M. Miyazaki, A. Osaka, N.-H. Huh, and K. Abe, Implantation of a New Porous Gelatin-Siloxane Hybrid into a Brain Lesion as a Potential Scaffold for Tissue Regeneration, *J. Cerebral Blood Flow and Metabolism*, **26**, 1263-1273 (2006).
- ⁸Y. Shirosaki, C. M. Botelho, M. A. Lopes, and J. D. Santos, Synthesis and Characterization of

- Chitosan-Silicate Hydrogel as Resorbable Vehicle for Bonelike® Bone Graft, *J. Nanosci. Nanotechnol.*, **8**, 1–6 (2008).
- ⁹Z. Z. Li, L. X. Wen, L. Shao, and J. F. Chen, Fabrication of Porous Hollow Silica Nanoparticles and their Applications in Drug Release Control, *J. Control. Release*, **98**, 245-254 (2004).
- ¹⁰Z. Q. Ye, M. Q. Tan, G. L. Wang, and J. L. Yuan, Development of Functionalized Terbium Fluorescent Nanoparticles for Antibody Labeling and Time-resolved Fluoroimmunoassay Application, *Talanta*, **65**, 206-210 (2005).
- ¹¹M. Arroyo-Hernández, R. J. Martín-Palma, J. Pérez-Rigueiro, J. P. García-Ruiz, J. L. García-Fierro, and J. M. Martínez-Duart, Biofunctionalization of Surfaces of Nanostructured Porous Silicon, *Materials Science and Engineering: C*, **23**, 697-701 (2003).
- ¹²X. Li, Y. He, and M. T. Swihart, Surface Functionalization of Silicon Nanoparticles Produced by Laser-Driven Pyrolysis of Silane Followed by HF-HNO₃ Etching, *Langmuir*, **20**, 4720-4727 (2004).
- ¹³P.-J. Li, C. Ohtsuki, T. Kokubo, K. Nakanishi, N. Soga, T. Nakamura, T. Yamamuro, Apatite Formation Induced by Silica Gel in a Simulated Body Fluid, *J. Am. Ceram. Soc.*, **75**, 2094-97 (1992).
- ¹⁴K. Nakanishi, Pore Structure Control of Silica Gels Based on Phase Separation, *J. Porous Mat.*, **4**, 67-112 (1997).
- ¹⁵T. Kokubo and H. Takadama, How useful is SBF in predicting in vivo Bone Bioactivity? *Biomaterials*, **27**, 2907–2915 (2006).
- ¹⁶L. Ren, K. Tsuru, S. Hayakawa, and A. Osaka, Sol-Gel Preparation and in vitro Deposition of Apatite on Porous Gelatin-Siloxane Hybrids, *J. Non-Cryst. Solids*, **285**, 116-122 (2001).
- ¹⁷K. Tsuru, Y. Aburatani, T. Yabuta, S. Hayakawa, C. Ohtsuki, and A. Osaka, Synthesis and In Vitro Behavior of Organically Functionalized Silicate Containing Ca Ions, *J. Sol-Gel Sci. Technol.*, **21**, 89-96 (2001).
- ¹⁸W. Stöber, A. Fink, and E. Bohn, Controlled Growth of Monodisperse Silica Spheres in the Micron Size Range, *J. Colloid Interf. Sci.*, **26**, 62-69 (1968).
- ¹⁹S. Chen, A. Osaka, S. Hayakawa, K. Tsuru, E. Fujii, and K. Kawabata, Novel One-Pot Sol-Gel Preparation of Amino-Functionalized Silica Nanoparticles, *Chem. Lett.*, **37**, 1170-1171 (2008).
- ²⁰S. A. Carroll, R. S. Maxwell, W. Bourcier, S. Martin, and S. Hulse, Evaluation of Silica-Water Surface Chemistry Using NMR Spectroscopy, *Geochim. Cosmochim. Acta.*, **66**, 913-26 (2002).
- ²¹F. Szurdoki, E. Trousdale, B. Ward, S. J. Gee, B. D. Hammock, and D. G. Gilchrist, Synthesis of Protein Conjugates and Development of Immunoassays for AAL Toxins, *J. Agric. Food Chem.*, **44**, 1796-1803 (1996).
- ²²J. S. Mao, H. F. Liu, Y. J. Yin, and K. D. Yao, The Properties of Chitosan-Gelatin Membranes and Scaffolds Functionalized with Hyaluronic Acid by Different Methods, *Biomaterials*, **24**, 1621-1629 (2003).
- ²³G. H. Bogush and C. F. Zukoski, Studies of the Kinetics of Precipitation of Uniform Silica Particles Through the Hydrolysis and Condensation of Silicon Alkoxides, *J. Colloid Interf. Sci.*, **142**, 1-18 (1991).
- ²⁴G. H. Bogush and C. F. Zukoski, Uniform Silica Particle Precipitation: an Aggregative Growth Model, *J. Colloid Interf. Sci.*, **142**, 19-34 (1991).
- ²⁵D. L. Green, J. S. Lin, Y. F. Lam, M. Z. Hu, D. W. Schaefer, and M. T. Harris, Size, Volume, Fraction, and Nucleation of Stöber Silica Nanoparticles, *J. Colloid Interf. Sci.*, **266**, 346-358 (2003).
- ²⁶H. Choi and I.-W. Chen, Surface-modified Silica Colloid for Diagnostic Imaging, *J. Colloid Interf. Sci.*, **258**, 435-437 (2003).
- ²⁷R. Zerrouk, A. Foissy, R. Mercier, and Y. Chevallier, J.-C. Morawski, Study of Ca²⁺ Induced Silica Coagulation by Small-Angle Scattering, *J. Colloid Interface Sci.*, **139**, 20-29 (1990).
- ²⁸S. Chen, A. Osaka, S. Hayakawa, K. Tsuru, E. Fujii, and K. Kawabata, Microstructure Evolution in Stöber-Type Silica Nanoparticles and their in vitro Apatite Deposition, *J. Sol-Gel Sci. Technol.*, **48**,

322–335 (2008).

²⁹⁾J. Van Muylder, J. Besson, W. Kunz and M. Porubaix, in *Atlas of Electrochemical Equilibria in Aqueous Solutions*, ed. M. Pourbaix, Pergamon Press, Oxford, Chapter IV, §17.2

³⁰⁾L. L. Hench and J. K. West, The Sol-Gel Process, *Chem. Rev.*, **90**, 33-72 (1990).

³¹⁾A. van Blaaderen and A. Vrij, Synthesis and Characterization of Monodisperse Colloidal Organo-Silica Spheres, *J. Colloid Interf. Sci.*, **156**, 1-18 (1993).

